

Supplementary Data

***In-situ desalination-coupled electrolysis with concurrent one-step-synthesis
of value-added chemicals***

Byeong-ju Kim,¹ Ho Kyong Shon,² Dong Suk Han,³ and Hyunwoong Park^{1,*}

¹*School of Energy Engineering, Kyungpook National University, Daegu 41566, Republic of Korea*

²*School of Civil and Environmental Engineering, University of Technology, Sydney, Post Box 129, Broadway, Sydney, NSW 2007, Australia*

³*Center for Advanced Materials and Department of Chemical Engineering, Qatar University, P.O. Box 2713, Doha, Qatar*

*To whom correspondence should be addressed:

(D.S. Han) E-mail: dhan@qu.edu.qa

(H. Park) E-mail: hwp@knu.ac.kr

Table S1. Elemental (metal) fractions of NiFe-LDH and NiMo catalysts estimated by XPS, SEM-EDS, and STEM.

Sample	Element	Elemental fraction (%)		
		XPS	SEM-EDS	STEM
As-deposited	Ni	73.6	31.2	68.4
NiFe-LDH	Fe	26.4	68.8	31.6
Post-anodized	Ni	66.9	34.3	70.2
NiFe-LDH	Fe	33.1	65.7	29.8
NiMo	Ni	81.7	89.6	-
	Mo	18.3	10.4	-

Table S2. Performance comparison of water splitting catalysts in literature.

Catalysts (anode cathode)	Support (anode cathode)	Conditions (anolyte membrane catholyte)	E_{cell} (V)	Durability (h)	Reference
NiFe-LDH NiMo	Ni foam Ni foam	1 M KOH BPM 1 M H₂SO₄	1.57 @10 mA cm⁻²	20	This work
NiFe-LDH CoP	Ni foam Ti foil	1 M KOH BPM 0.5 M H ₂ SO ₄	1.63 @10 mA cm ⁻²	90	[1]
Co-Ni-P Co-Ni-P	Ni foam Ni foam	1 M NaOH BPM 0.5 M H ₂ SO ₄	1.55 @10 mA cm ⁻²	25	[2]
CoP-CoTe ₂ CoP-CoTe ₂	Carbon paper carbon paper	1 M KOH BPM 0.5 M H ₂ SO ₄	1.72 @10 mA cm ⁻²	100	[3]
LSC/K-MoSe ₂ LSC/K-MoSe ₂	Ni foam Ni foam	1 M KOH	1.59 @10 mA cm ⁻²	- (LSV)	[4]
NiFe-LDH@NiCoP NiFe- LDH@NiCoP	Ni foam Ni foam	1 M KOH	1.57 @10 mA cm ⁻²	100	[5]
Ni ₂ P@NiFe hydroxide Ni ₂ P@NiFe hydroxide	Ni foam Ni foam	1 M KOH	1.51 @10 mA cm ⁻²	100	[6]
Ni/NiS/NC Ni/NiS/NC	Glassy carbon glassy carbon	1 M KOH	1.61 @10 mA cm ⁻²	25	[7]
MoS ₂ @Ni _{0.96} S MoS ₂ @Ni _{0.96} S	Ni foam Ni foam	1 M KOH	1.68 @10 mA cm ⁻²	15	[8]
RuTe ₂ RuTe ₂	Glassy carbon glassy carbon	1 M KOH	1.57 @10 mA cm ⁻²	20	[9]
RuCu RuCu	Glassy carbon glassy carbon	1 M KOH	1.50 @10 mA cm ⁻²	12	[10]
NiSe ₂ -Ni ₂ P NiSe ₂ -Ni ₂ P	Ni foam Ni foam	1 M KOH	1.50 @10 mA cm ⁻²	- (LSV)	[11]

NiCo ₂ O ₄ @FeOOH NiCo ₂ O ₄ @FeOOH	Ni foam Ni foam	1 M KOH	1.52 @10 mA cm ⁻²	- (LSV)	[12]
NiCo ₂ O ₄ NiCo ₂ O ₄	Ni foam Ni foam	1 M NaOH	1.65 @10 mA cm ⁻²	32 h	[13]
FeWO ₄ -Ni ₃ S ₂ @C FeWO ₄ -Ni ₃ S ₂ @C	Ni foam Ni foam	1 M KOH	1.51 @10 mA cm ⁻²	- (LSV)	[14]
Fe ₂ O ₃ /CuO Fe ₂ O ₃ /CuO	Ni foam Ni foam	1 M KOH	1.49 @10 mA cm ⁻²	10 h	[15]

References

- [1] J.S. Luo, D.A. Vermaas, D.Q. Bi, A. Hagfeldt, W.A. Smith, M. Gratzel, Bipolar Membrane-Assisted Solar Water Splitting in Optimal pH, *Adv. Energy Mater.*, 6 (2016) 1600100. <https://doi.org/10.1002/aenm.201600100>
- [2] J.Y. Xu, I. Amorim, Y. Li, J.J. Li, Z.P. Yu, B.S. Zhang, A. Araujo, N. Zhang, L.F. Liu, Stable overall water splitting in an asymmetric acid/alkaline electrolyzer comprising a bipolar membrane sandwiched by bifunctional cobalt-nickel phosphide nanowire electrodes, *Carbon Energy*, 2 (2020) 646-655. <https://doi.org/10.1002/cey2.56>
- [3] I. Amorim, J.Y. Xu, N. Zhang, Z.P. Yu, A. Araujo, F. Bento, L.F. Liu, Dual-phase CoP-CoTe₂ nanowires as an efficient bifunctional electrocatalyst for bipolar membrane-assisted acid-alkaline water splitting, *Chem. Eng. J.*, 420 (2021) 130454. <https://doi.org/10.1016/j.cej.2021.130454>
- [4] N.K. Oh, J. Seo, S. Lee, H.J. Kim, U. Kim, J. Lee, Y.K. Han, H. Park, Highly efficient and robust noble-metal free bifunctional water electrolysis catalyst achieved via complementary charge transfer, *Nat. Commun.*, 12 (2021) 4606. <https://doi.org/10.1038/s41467-021-24829-8>
- [5] H.J. Zhang, X.P. Li, A. Hahnel, V. Naumann, C. Lin, S. Azimi, S.L. Schweizer, A.W. Maijenburg, R.B. Wehrspohn, Bifunctional Heterostructure Assembly of NiFe LDH Nanosheets on NiCoP Nanowires for Highly Efficient and Stable Overall Water Splitting, *Adv. Funct. Mater.*, 28 (2018) 1706847. <https://doi.org/10.1002/adfm.201706847>
- [6] F.S. Zhang, J.W. Wang, J. Luo, R.R. Liu, Z.M. Zhang, C.T. He, T.B. Lu, Extraction of nickel from NiFe-LDH into Ni₂P@NiFe hydroxide as a bifunctional electrocatalyst for efficient overall water splitting, *Chem. Sci.*, 9 (2018) 1375-1384. <https://doi.org/10.1039/C7SC04569G>
- [7] J.T. Ding, S. Ji, H. Wang, H.J. Gai, F.S. Liu, V. Linkov, R.F. Wang, Mesoporous nickel-sulfide/nickel/N-doped carbon as HER and OER bifunctional electrocatalyst for water electrolysis, *Int. J. Hydron. Energy*, 44 (2019) 2832-2840. <https://doi.org/10.1016/j.ijhydene.2018.12.031>

- [8] S.H. Liu, B.Y. Li, S.V. Mohite, P. Devaraji, L.Q. Mao, R.M. Xing, Ultrathin MoS₂ nanosheets in situ grown on rich defective Ni_{0.96}S as heterojunction bifunctional electrocatalysts for alkaline water electrolysis, *Int. J. Hydrog. Energy*, 45 (2020) 29929-29937. <https://doi.org/10.1016/j.ijhydene.2020.08.034>
- [9] B. Tang, X.D. Yang, Z.H. Kang, L.G. Feng, Crystallized RuTe₂ as unexpected bifunctional catalyst for overall water splitting, *Appl. Catal. B*, 278 (2020) 119281. <https://doi.org/10.1016/j.apcatb.2020.119281>
- [10] Q. Yao, B.L. Huang, N. Zhang, M.Z. Sun, Q. Shao, X.Q. Huang, Channel-Rich RuCu Nanosheets for pH-Universal Overall Water Splitting Electrocatalysis, *Angew. Chem. Int. Ed.*, 58 (2019) 13983-13988. <https://doi.org/10.1002/ange.201908092>
- [11] P.Y. Wang, Z.H. Pu, W.Q. Li, J.W. Zhu, C.T. Zhang, Y.F. Zhao, S.C. Mu, Coupling NiSe₂-Ni₂P heterostructure nanowrinkles for highly efficient overall water splitting, *J. Catal.*, 377 (2019) 600-608. <https://doi.org/10.1016/j.jcat.2019.08.005>
- [12] M. Li, L.M. Tao, X. Xiao, X.W. Lv, X.X. Jiang, M.K. Wang, Z.Q. Peng, Y. Shen, Core-Shell Structured NiCo₂O₄@FeOOH Nanowire Arrays as Bifunctional Electrocatalysts for Efficient Overall Water Splitting, *ChemCatChem*, 10 (2018) 4119-4125. <https://doi.org/10.1002/cctc.201800606>
- [13] X.H. Gao, H.X. Zhang, Q.G. Li, X.G. Yu, Z.L. Hong, X.W. Zhang, C.D. Liang, Z. Lin, Hierarchical NiCo₂O₄ Hollow Microcuboids as Bifunctional Electrocatalysts for Overall Water-Splitting, *Angew. Chem. Int. Ed.*, 55 (2016) 6290-6294. <https://doi.org/10.1002/anie.201600525>
- [14] Z.L. Wang, G.F. Qian, T.Q. Yu, J.L. Chen, F. Shen, L. Luo, Y.J. Zou, S.B. Yin, Carbon encapsulated FeWO₄-Ni₃S₂ nanosheets as a highly active catalyst for overall water splitting at large current density, *Chem. Eng. J.*, 434 (2022) 134669. <https://doi.org/10.1016/j.cej.2022.134669>
- [15] F. Hu, D.S. Yu, M. Ye, H. Wang, Y.A. Hao, L.Q. Wang, L.L. Li, X.P. Han, S.J. Peng, Lattice-Matching Formed Mesoporous Transition Metal Oxide Heterostructures Advance Water Splitting by Active Fe-O-Cu Bridges, *Adv. Energy Mater.*, 12 (2022) 2200067. <https://doi.org/10.1002/aenm.202200067>

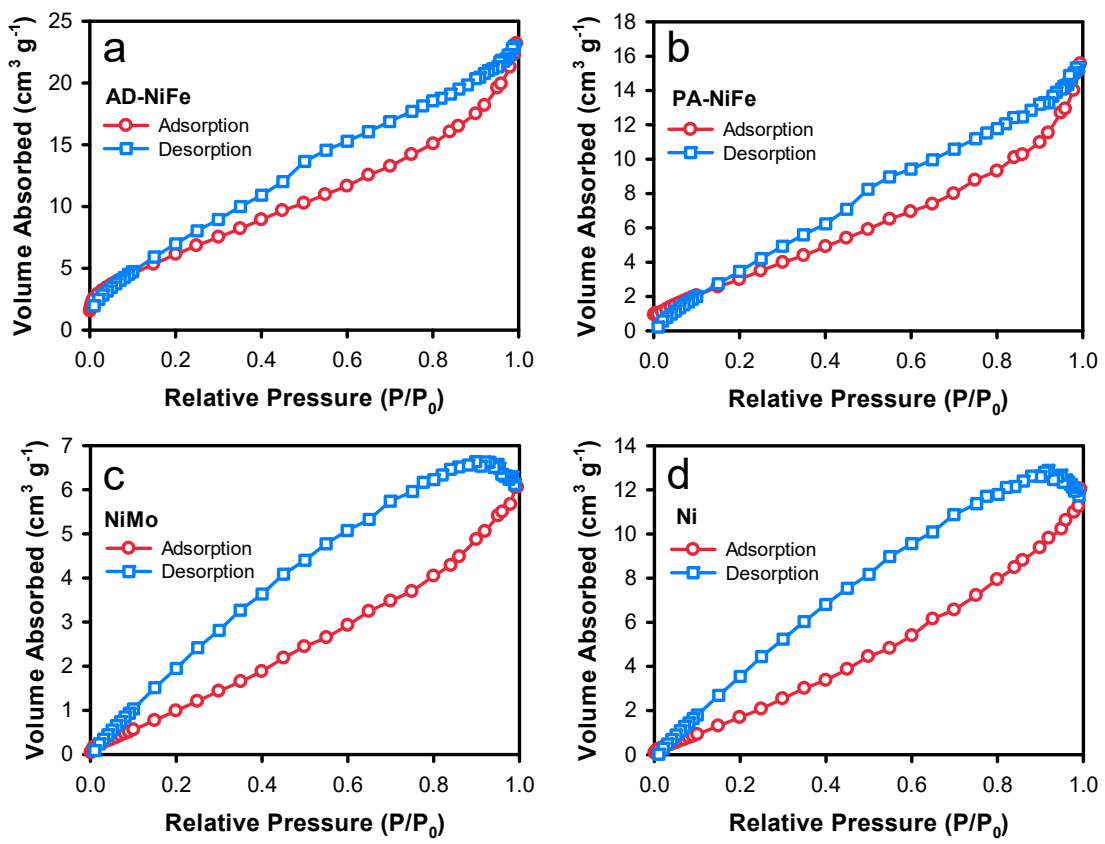


Figure S1. N₂ adsorption and desorption isotherms of (a) as-deposited NiFe-LDH (AD-NiFe), (b) post-anodized NiFe-LDH (PA-NiFe), (c) NiMo, and (d) Ni substrate.

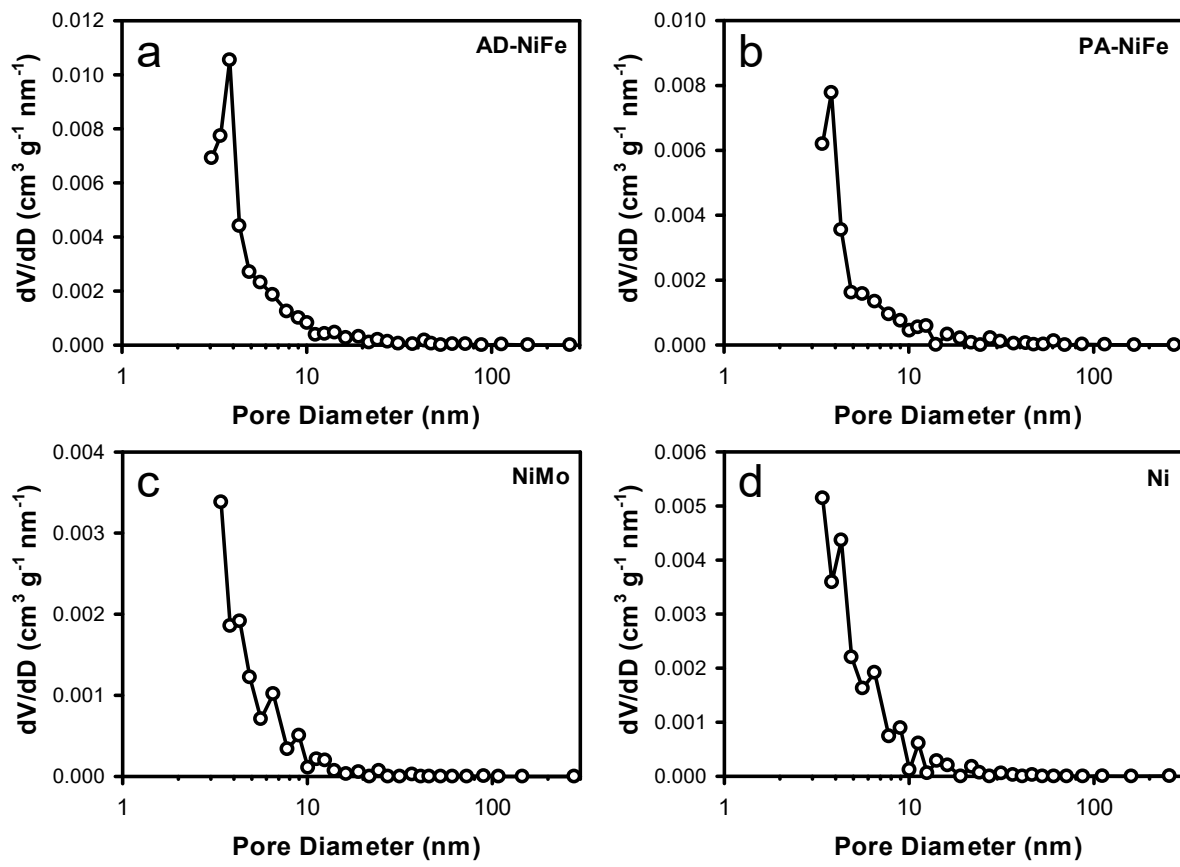


Figure S2. Pore diameter distributions of (a) as-deposited NiFe (AD-NiFe), (b) post-anodized NiFe (PA-NiFe), (c) NiMo, and (d) Ni substrate.

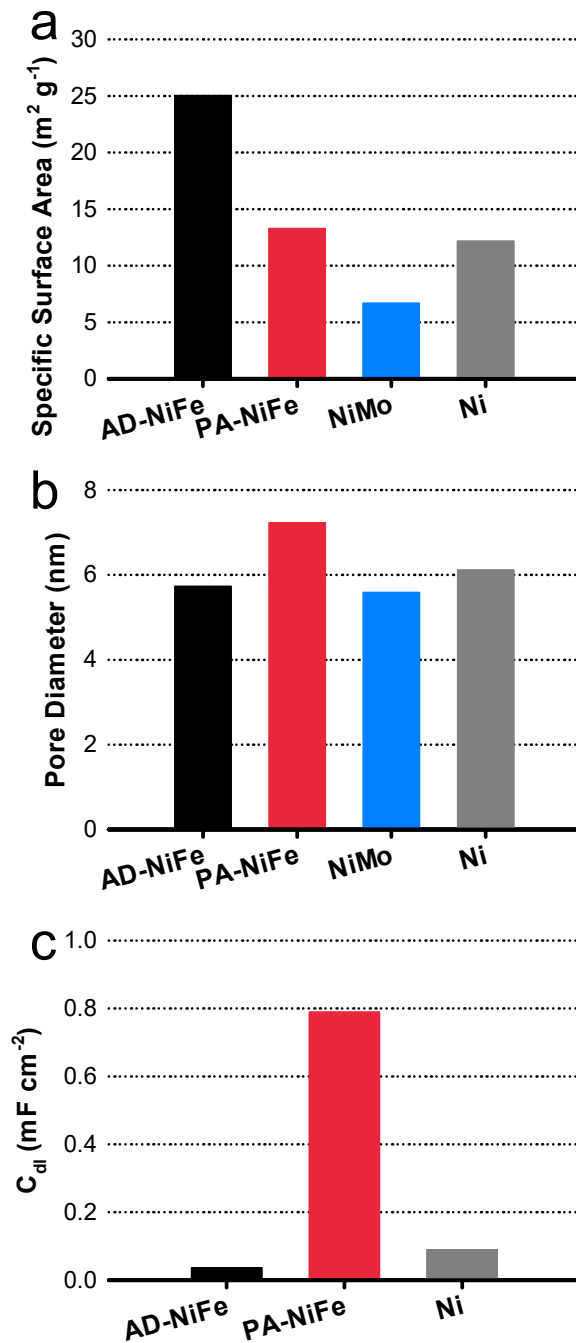


Figure S3. (a) Specific surface areas (BET method), (b) average pore diameters (BJH method), and (c) electrochemical double-layer capacitance (C_{dl}) of as-deposited NiFe-LDH (AD-NiFe), post-anodized NiFe (PA-NiFe), NiMo, and Ni substrate. Electrolytes for NiFe and Ni substrate: 1 M KOH. Electrolyte for NiMo: 1 M H_2SO_4 . C_{dl} of NiMo was not obtained due to high Faradaic currents in the acidic solution.

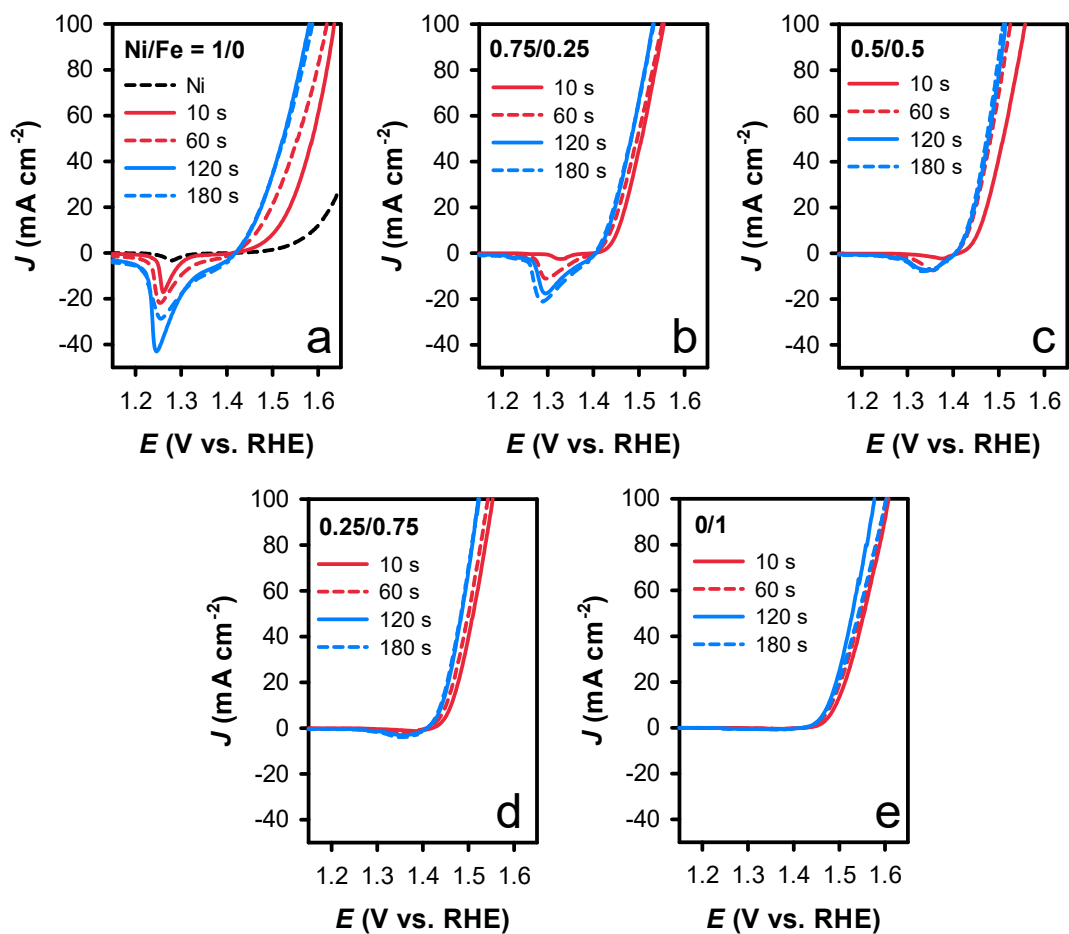
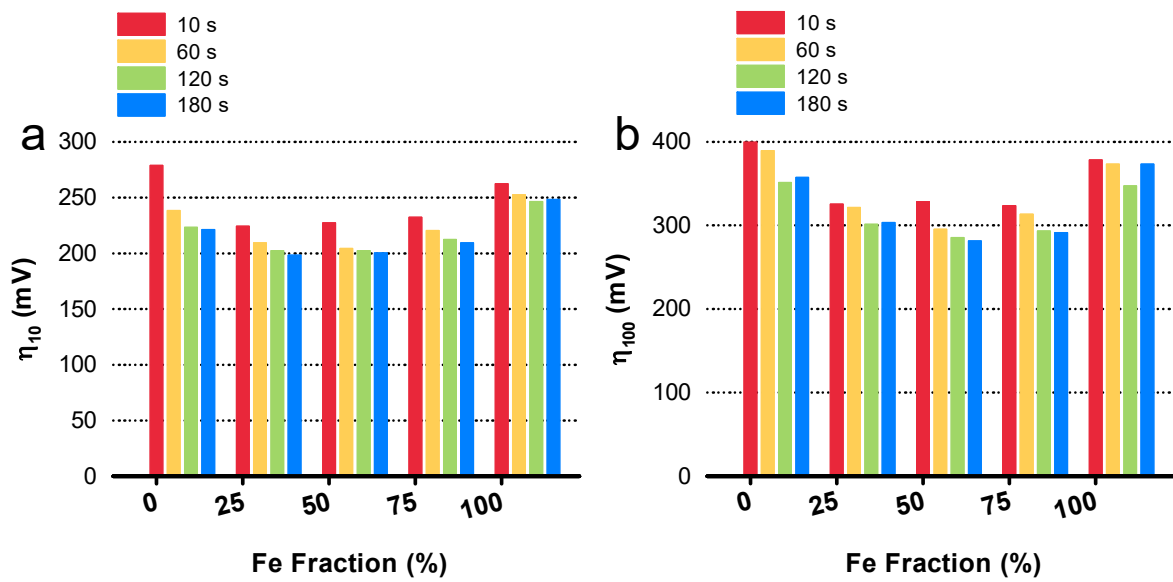


Figure S4. Linear sweep voltammograms of NiFe-LDH electrodes deposited at various Ni/Fe ratios and deposition time.



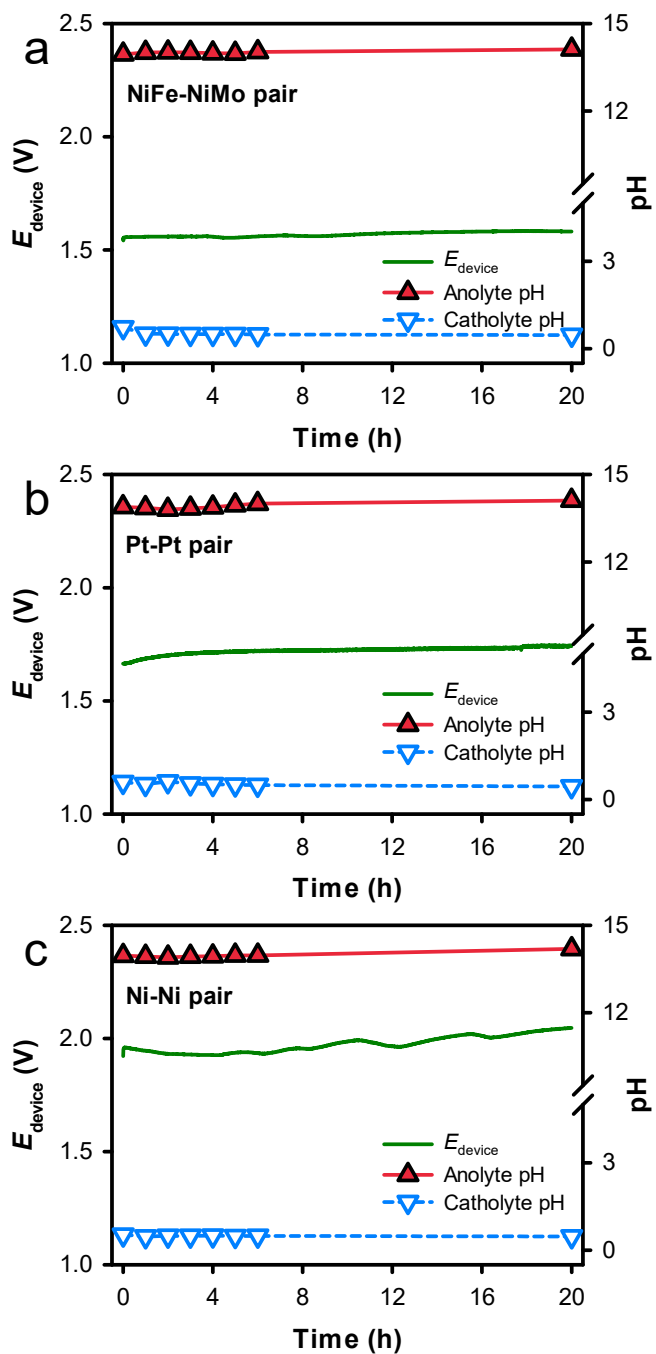


Figure S6. Changes in E_{device} and electrolyte pH values with time at $J = 10 \text{ mA cm}^{-2}$ in two-cell devices divided by BPMs with anolyte of 1 M KOH and catholyte of 1 M H_2SO_4 . (a) NiFe-LDH anode and NiMo cathode pair, (b) Pt anode-Pt cathode pair, and (c) Ni anode-Ni cathode pair.

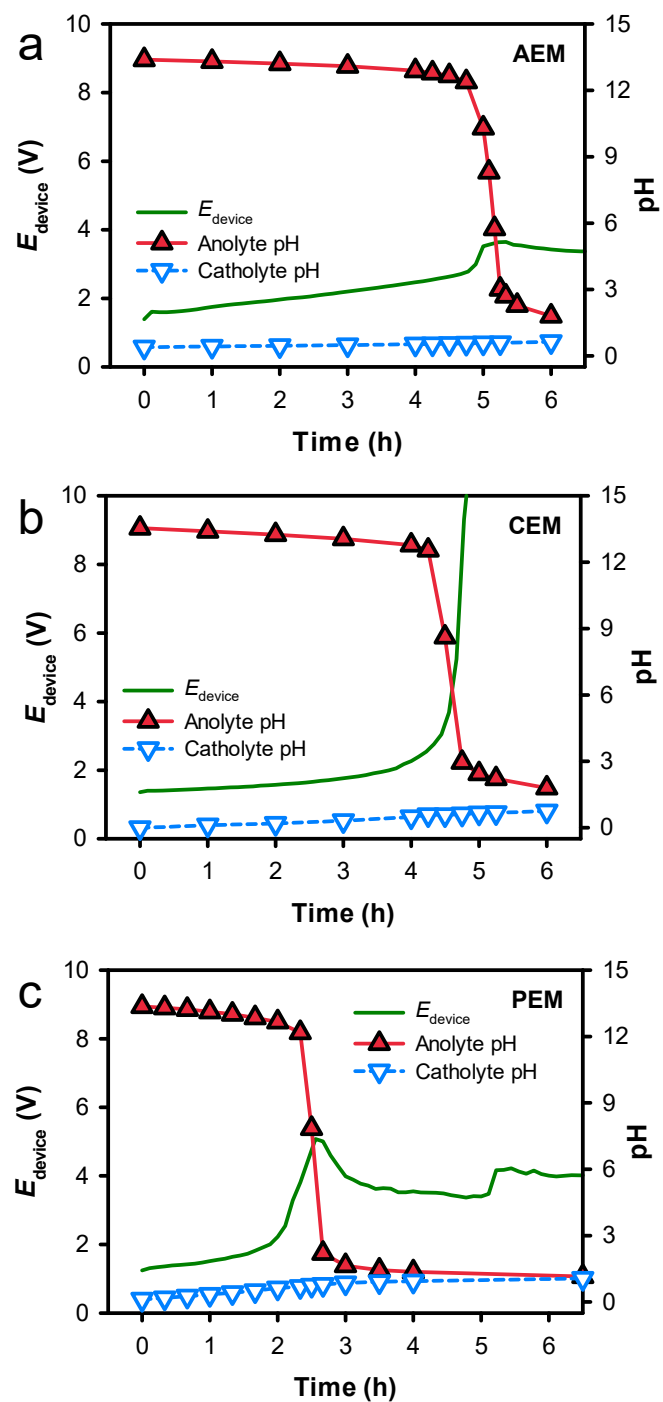


Figure S7. Changes in E_{device} and electrolyte pH values with NiFe-LDH anode and NiMo cathode pairs in two-cell devices divided by (a) an AEM, (b) a CEM, and (c) a PEM with anolyte of 1 M KOH and catholyte of 1 M H₂SO₄ at $J = 100 \text{ mA cm}^{-2}$.

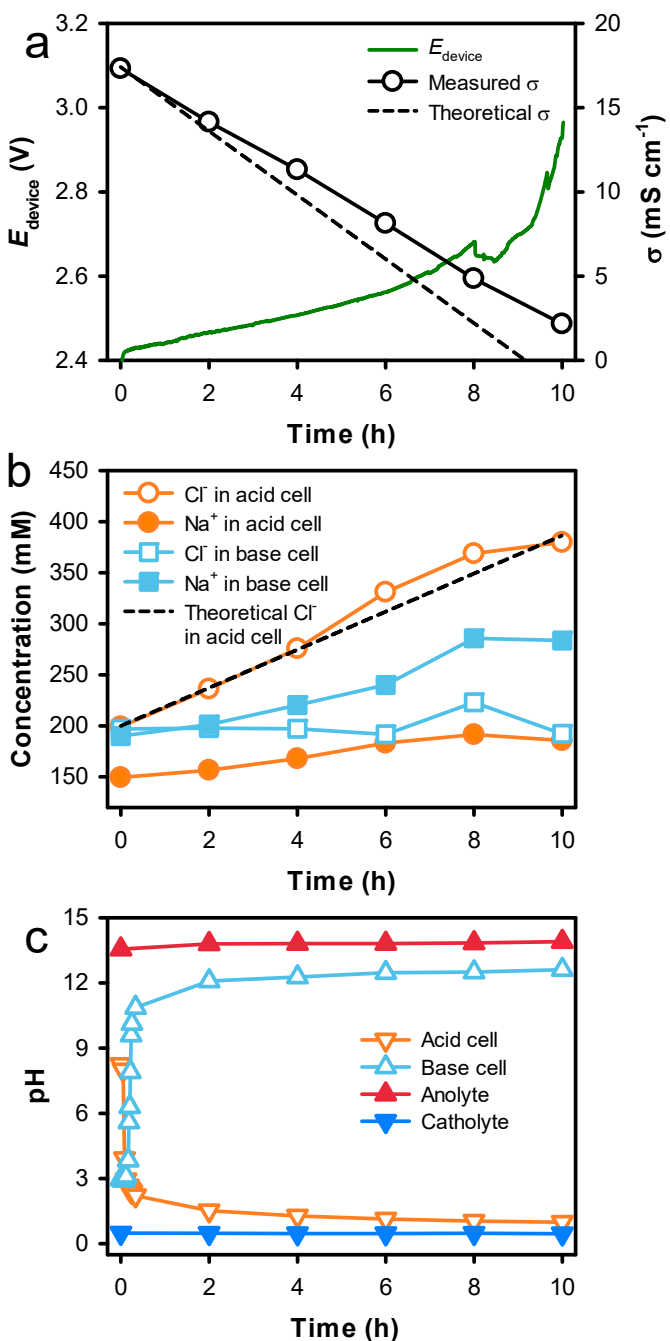


Figure S8. A desalination-coupled electrocatalytic unit device with NiFe-LDH anode and NiMo cathode at $J = 10 \text{ mA cm}^{-2}$ (Case Study II in Table 1). The device configuration is the same as that of Case Study I, except for acid cell (0.2 M NaCl) and base cell (0.2 M NaCl). For the device construction, see Scheme 1b. (a) Changes in E_{device} and ionic conductivity (σ) of saline water with electrolysis time. (b) Changes in concentrations of desalinated ions (Cl^- and Na^+). (c) Changes in pH values in the solutions in the acid and base cells, and electrolytes.

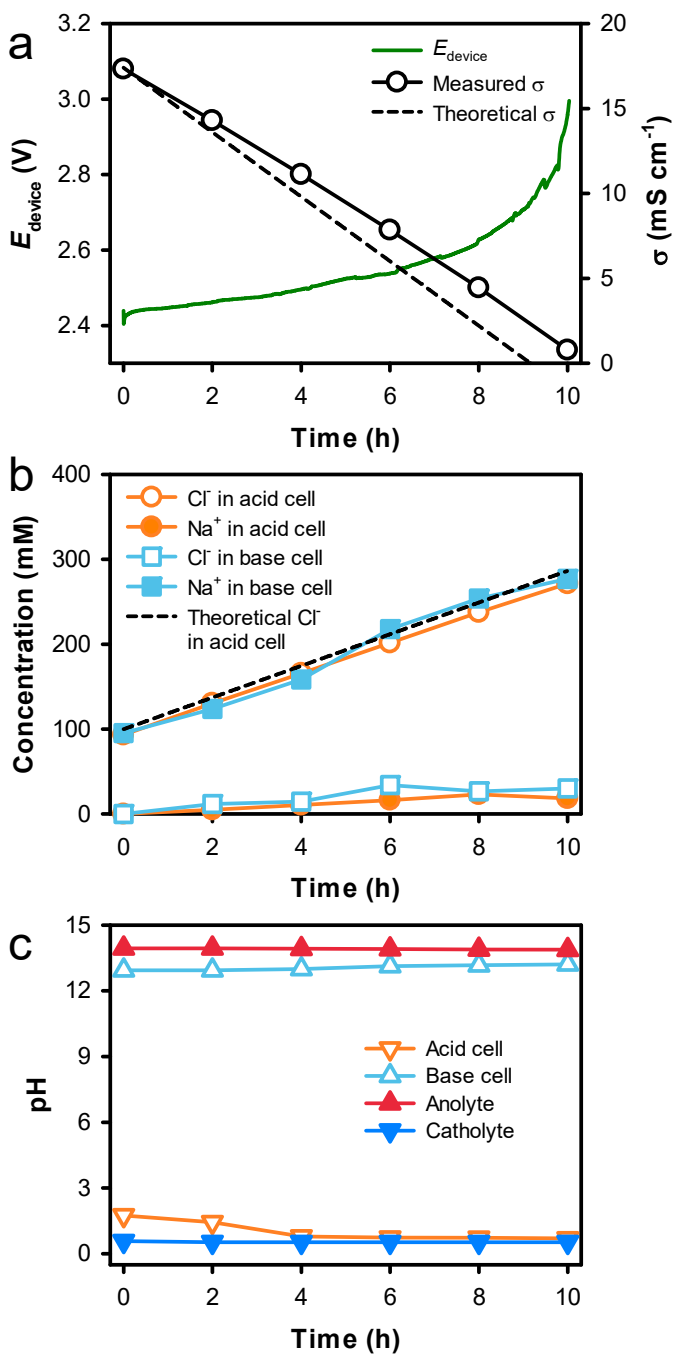


Figure S9. A desalination-coupled electrocatalytic unit device with NiFe-LDH anode and NiMo cathode at $J = 10 \text{ mA cm}^{-2}$ (Case Study III in Table 1). The device configuration is the same as that of Case Study I, except for acid cell (0.1 M HCl) and base cell (0.1 M NaOH). For the device construction, see Scheme 1b. (a) Changes in E_{device} and ionic conductivity (σ) of saline water with electrolysis time. (b) Changes in concentrations of desalted ions (Cl^- and Na^+). (c) Changes in pH values in the solutions in the acid and base cells, and electrolytes.

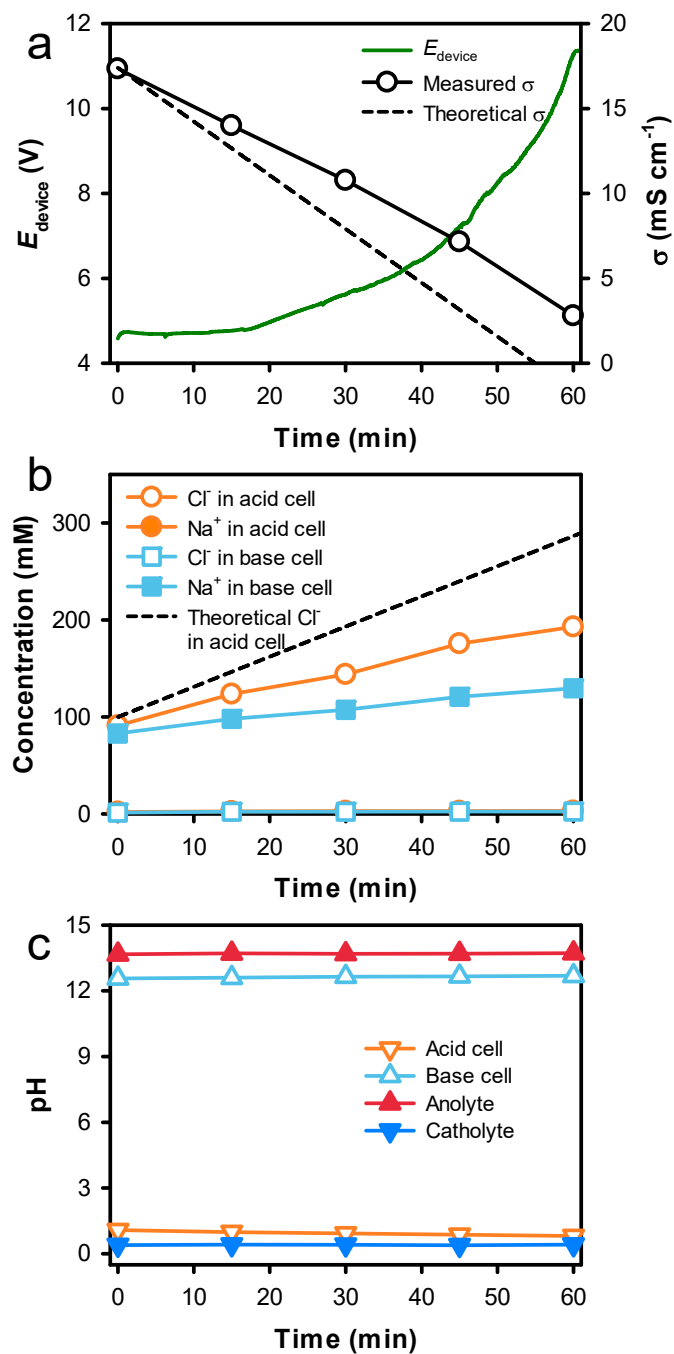


Figure S10. A desalination-coupled electrocatalytic unit device with NiFe-LDH anode and NiMo cathode at $J = 100 \text{ mA cm}^{-2}$ (Case Study IV in Table 1). The other conditions are the same as those in Figure S9. (a) Changes in E_{device} and ionic conductivity (σ) of saline water with electrolysis time. (b) Changes in concentrations of desalinated ions (Cl⁻ and Na⁺). (c) Changes in pH values in the solutions in the acid and base cells, and electrolytes.

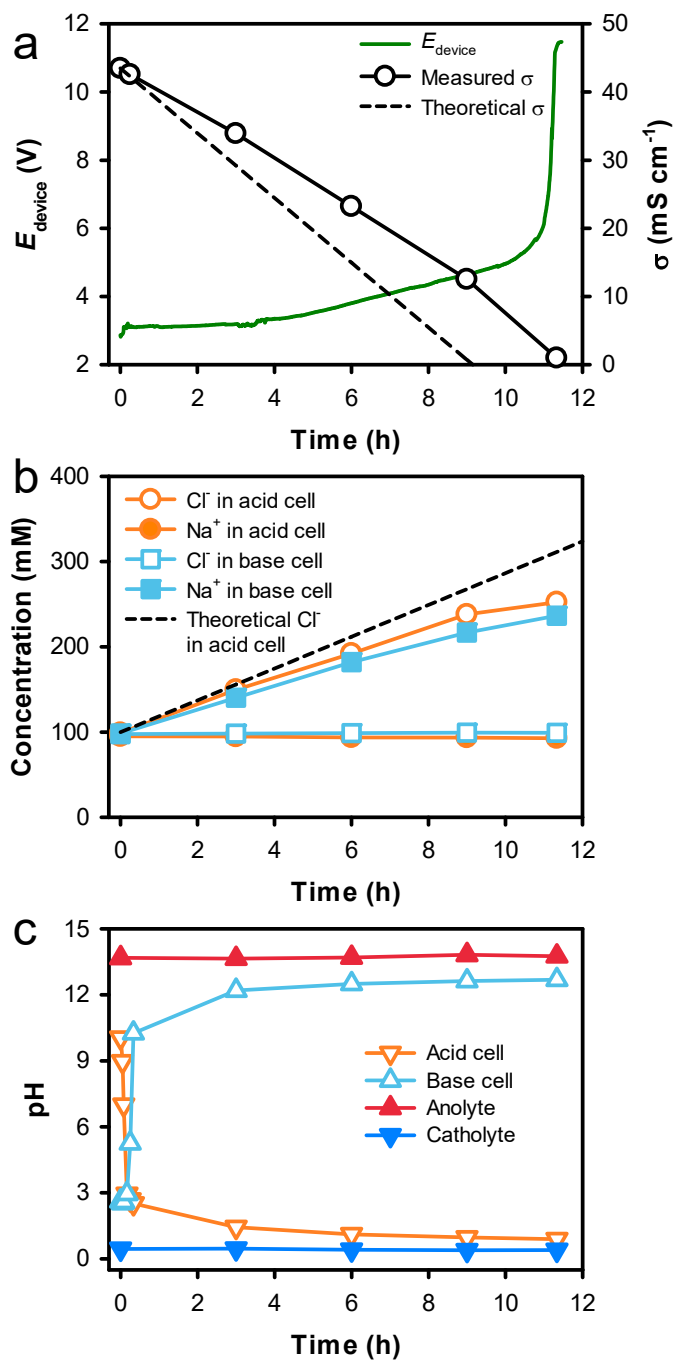


Figure S11. A five-desalination cell array-coupled electrocatalysis with desalination cell (seawater, salinity 36 g L^{-1}). For device configuration and conditions, refer to Case Study VI in Table 1. (a) Changes in E_{device} and ionic conductivity (σ) of saline water with electrolysis time. The dashed line represents the theoretical σ based on J . (b) Changes in concentrations of desalinated ions (Cl^- and Na^+). The dashed line represents the theoretical Cl^- concentration in the acid cell. (c) Changes in pH values in the solutions in the acid and base cells, and electrolytes.